Phenothiazines inhibit S100A4 function by inducing protein oligomerization

Vladimir N. Malashkevich[a], Natalya G. Dulyaninova[a], Udupi A. Ramagopal[a], Melissa A. Liriano[b], Kristen M. Varney[b], David Knight[a2], Michael Brenowitz[a], David J. Weber[b], Steven C. Almo[a], and Anne R. Bresnick[a,1]

[a]Department of Biochemistry, Albert Einstein College of Medicine, 1300 Morris Park Avenue, Bronx, NY 10461; and [b]Department of Biochemistry and Molecular Biology, University of Maryland School of Medicine, 108 North Greene Street, Baltimore, MD, 21201

Edited by Gregory A. Petsko, Brandeis University, Waltham, MA, and approved April 1, 2010 (received for review November 25, 2009)

S100A4, a member of the S100 family of Ca^{2+}-binding proteins, regulates carcinoma cell motility via interactions with myosin-IIA. Numerous studies indicate that S100A4 is not simply a marker for metastatic disease, but rather has a direct role in metastatic progression. These observations suggest that S100A4 is an excellent target for therapeutic intervention. Using a unique biosensor-based assay, trifluoperazine (TFP) was identified as an inhibitor that disrupts the S100A4/myosin-IIA interaction. To examine the interaction of S100A4 with TFP, we determined the 2.3 Å crystal structure of human Ca^{2+}-S100A4 bound to TFP. Two TFP molecules bind within the hydrophobic target binding pocket of Ca^{2+}-S100A4 with no significant conformational changes observed in the protein upon complex formation. NMR chemical shift perturbations are consistent with the crystal structure and demonstrate that TFP binds to the target binding cleft of S100A4 in solution. Remarkably, TFP binding results in the assembly of five Ca^{2+}-S100A4/TFP dimers into a tightly packed pentameric ring. Within each pentamer most of the contacts between S100A4 dimers occurs through the TFP moieties. The Ca^{2+}-S100A4/prochlorperazine (PCP) complex exhibits a similar pentameric assembly. Equilibrium sedimentation and cross-linking studies demonstrate the cooperative formation of a similarly sized S100A4/TFP oligomer in solution. Assays examining the ability of TFP to block S100A4-mediated disassembly of myosin-IIA filaments demonstrate that significant inhibition of S100A4 function occurs only at TFP concentrations that promote S100A4 oligomerization. Together these studies support a unique mode of inhibition in which phenothiazines disrupt the S100A4/myosin-IIA interaction by sequestering S100A4 via small molecule-induced oligomerization.

calcium | X-ray crystallography | NMR | small molecule inhibitor | metastasis

The S100 proteins, of which there are more than 20 members, are characterized by their solubility in 100% saturated ammonium sulfate (1 and 2). Each S100 family member contains two Ca^{2+}-binding loops; a C-terminal "typical" EF-hand comprised of 12 residues and an N-terminal pseudo EF-hand consisting of 14 residues. The basic organization of the S100 proteins is a symmetric, antiparallel homodimer, in which the N- and C- terminal helices (helices 1 and 4) from each subunit interact to form a stable four helix bundle that serves as the dimer interface. Calcium binding to the C-terminal typical EF-hand significantly alters the angle between helices 3 and 4, which flank the C-terminal Ca^{2+}-binding loop, and exposes a hydrophobic cleft that constitutes a binding surface for target proteins (3–5). Thus the S100 proteins operate as calcium-activated switches that bind and regulate the activity of diverse protein targets.

S100 proteins are expressed in a tissue and cell specific manner. Elevated expression of individual family members is associated with a number of human pathologies, including cardiomyopathies, cancer, neurodegeneration, and inflammatory disorders (1 and 6). For S100A4, increased protein expression correlates with a high incidence of metastasis and poor prognosis for a number of different cancers (7 and 8). In addition, high S100A4 expression levels contribute to fibrotic and inflammatory diseases such as rheumatoid arthritis, cardiac hypertrophy, and kidney fibrosis (9 and 10). Given the contribution of S100A4 activity to a variety of human pathologies, it has received significant attention as a possible target for therapeutic intervention.

The disruption of S100A4 binding to its protein targets provides the most straightforward means for inhibiting S100A4 activity. S100A4, like other S100 family members, is reported to have multiple Ca^{2+}-dependent protein targets that include the cytoskeletal proteins nonmuscle myosin-IIA, tropomyosin, and F-actin (11–13), signaling proteins such as liprin β1 (14), the transcription factor p53 (15) and cell surface molecules annexin A2 and Tag7 (16 and 17). At this time there is little structural information on S100A4-target complexes (5), which will be needed for the development of S100A4-based therapies.

Using a biosensor that reports on the Ca^{2+}-activation status of S100A4, we previously identified several phenothiazines that block the Ca^{2+}-induced fluorescence increase of the biosensor in the low to midmicromolar range (18). Several phenothiazines, including trifluoperazine (TFP), block the ability of S100A4 to depolymerize myosin-IIA filaments. To examine the mechanism of TFP inhibition of S100A4, we determined the X-ray structure of the Ca^{2+}-S100A4/TFP complex. The structure shows that TFP binding results in the assembly of five Ca^{2+}-S100A4/TFP dimers into a tightly packed pentameric ring via interactions between the two TFP molecules located in the hydrophobic target binding pocket of Ca^{2+}-S100A4. PCP induces a similar pentameric assembly, suggesting a general mechanism for phenothiazine-mediated oligomerization. Biochemical and biophysical assays support the formation of a similarly sized Ca^{2+}-S100A4/TFP oligomer in solution, and demonstrate that significant inhibition of S100A4 activity occurs only at TFP concentrations that promote S100A4 oligomerization. We propose a unique mode of inhibition in which phenothiazines disrupt S100A4 activity via small molecule-induced oligomerization.

Results

Structure Determination. A molecular replacement search with the Ca^{2+}-activated human S100A4 dimeric structure (PDB 2Q91) (5) produced unique rotation and translation solutions corresponding to 10 S100A4 dimers in the asymmetric unit. In the final model, 95.8%, 3.5%, and 0.7% of residues are in favorable, allowed,

Author contributions: N.G.D., D.J.W., S.C.A., and A.R.B. designed research; V.M., N.G.D., U.A.R., M.A.L., K.M.V., D.K., M.B., and A.R.B. performed research; V.M., N.G.D., U.A.R., M.A.L., K.M.V., M.B., D.J.W., S.C.A., and A.R.B. analyzed data; and V.M., M.B., D.J.W., S.C.A., and A.R.B. wrote the paper.

The authors declare no conflict of interest.

This article is a PNAS Direct Submission.

Data deposition: The sequences reported in this article have been deposited in the Protein Data Bank, www.pdb.org (PDB ID codes 3KO0 and 3M0W).

[1]To whom correspondence should be addressed. E-mail: bresnick@aecom.yu.edu.

[2]Present address: Department of Biology and Biochemistry, University of Bath, Bath, BA2 7AY United Kingdom.

This article contains supporting information online at www.pnas.org/lookup/suppl/doi:10.1073/pnas.0913660107/-/DCSupplemental.

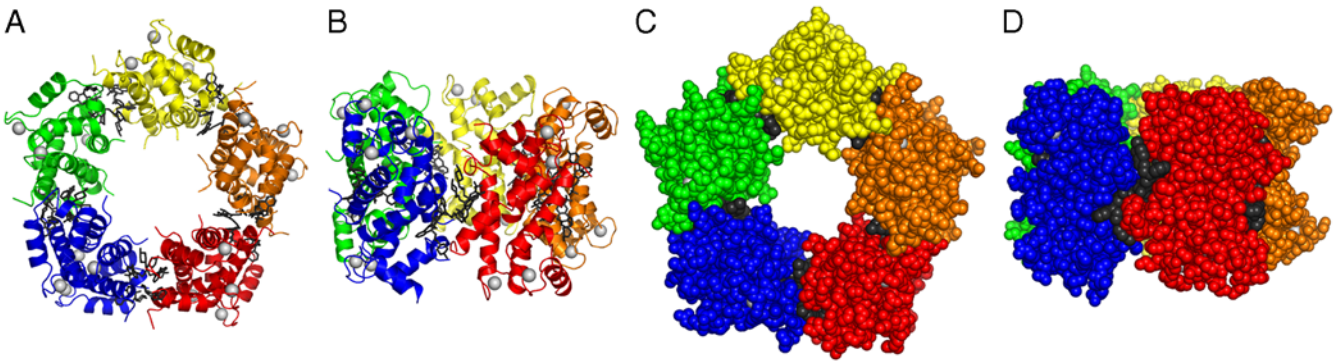

Fig. 1. Crystal packing of the Ca^{2+}-S100A4/TFP molecules. The protein dimers are arranged in a pentameric ring facilitated by TFP molecules (*dark gray*). (*A*) and (*B*) Ribbon diagrams showing top and side views of the pentamer, respectively; (*C*) and (*D*) Corresponding space filling models. Note the large solvent channel in the interior of the pentamer.

and generous areas of the Ramachandran plot, respectively (19) (Table S1). Residues with less favorable backbone conformations are located in the conformationally flexible loops and the C-terminal tail. Most of the key structural elements in the 20 independent chains in the asymmetric unit exhibit well defined electron density except for the most C-terminal residues (Asp95–Lys101) and the loop between helices 2 and 3 (Gly47–Glu52). Further structural description, discussion, and comparisons will be based on the structure of the S100A4 dimer comprised of subunits A and B since they display the most well defined electron density overall.

Quaternary Structure of Ca^{2+}-S100A4/TFP. S100 family proteins are typically homodimers; however higher-order oligomers can be formed under specific conditions (20–22). As described by us previously, Ca^{2+}-S100A4 dimers can assemble into a continuous superhelical arrangement due to the interaction of the C-terminal tail with the target peptide binding cleft of symmetry-related molecules (5). In the current crystal structure, TFP binding results in the assembly of five Ca^{2+}-S100A4/TFP dimers into a pentameric ring with a molecular point symmetry of 52 (Fig. 1). The asymmetric unit contains two independent copies of the pentamer. Each pentamer has inner and outer diameters of 25 and 85 Å, respectively and a thickness of 51 Å. Within each pentamer, many of the contacts between S100A4 dimers occur through the TFP moieties (Fig. 2*A*). In addition, direct contacts are observed between residues in the loop connecting helices 1 and 2 (Gly21–Lys26), and residues from the loop connecting helices 2 and 3 (Gly47–Glu52) in the symmetry-related molecule (Fig. 2*A*). These contacts may be modest due to the significant degree of disorder within the Gly47–Glu52 loop. Fig. 2*B* shows the two TFP molecules from subunit A interacting with symmetry-related molecule CD. The details of these interactions are described below.

Molecular Interactions Between TFP and Ca^{2+}-S100A4. In the crystal, two TFP molecules are bound per S100A4 subunit (four inhibitor molecules per dimer), and both inhibitor molecules are well defined in the electron density map (Fig. 3 *A*, *B*). The interactions of the two TFP molecules (defined TFP1 and TFP2) are summarized in Table S2. The phenothiazine moiety of TFP1(A) packs against the solvent exposed side of helix 4 with the trifluoromethyl group pointing towards the C terminus of the helix (Fig. 3*C*). These hydrophobic contacts involve the sidechains of Ile82(A), Met85(A), Cys86(A), and Phe89(A). The methylpiperazine ring protrudes towards the hinge region between helices 2 and 3, and contacts the sidechains of Ser44(A), Phe45(A), Leu46(A), and Gly47(A). There is a potential hydrogen bond (2.9 Å) between the piperazine ring atom N3 and the carbonyl oxygen of Phe45(A). The remaining interactions of TFP1(A) are with TFP2(A), three water molecules and the C-terminal residues of helix 4 from the symmetry-related molecule (Phe89(C), Phe93(C), and TFP1(C)) (Fig. 2*B*). TFP2(A) binds with its phenothiazine moiety packing against helix 4 (Ile82(A), Cys86(A), and Phe89(A)), residues in the loop between helices 2 and 3 (Leu42(A), Ser44(A), and Phe45(A)), and helix 1 of subunit B (Glu6(B), Leu9(B), and Asp10(B)). The methyl-piperazine ring of TFP2(A) interacts with the sidechains of the symmetry-related molecules (Cys86(C), Phe89(C), TFP2(C), Asp10(D), and Ser14 (D)) and eight water molecules. There are two potential hydrogen bonds (2.8 and 3.0 Å) between the piperazine ring atom N3

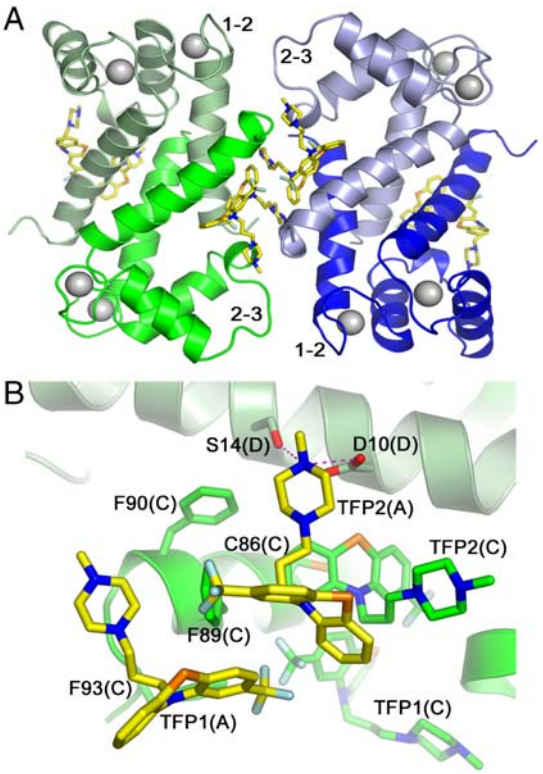

Fig. 2. View of the Ca^{2+}-S100A4/TFP dimer-to-dimer crystal interface. (*A*) Ribbon diagram of the AB (*light and dark blue*) and CD (*dark and light green*) S100A4 dimers. The Ca^{2+} atoms are shown as *light gray spheres*. The interhelical loops connecting helices 1 and 2 (*1–2*) and helices 2 and 3 (*hinge*), which are involved in crystal contacts, are indicated. (*B*) TFP interactions with the symmetry-related molecule. View from subunit A (*light blue*) towards CD dimer. The two TFP molecules (TFP1(*A*) and TFP2(*A*)) bound to subunit A are shown in *yellow*. Helix 4 of subunit C is *dark green* and helix 1 of subunit D is *light green*. Hydrogen bonds are shown as *dashed pink lines*.

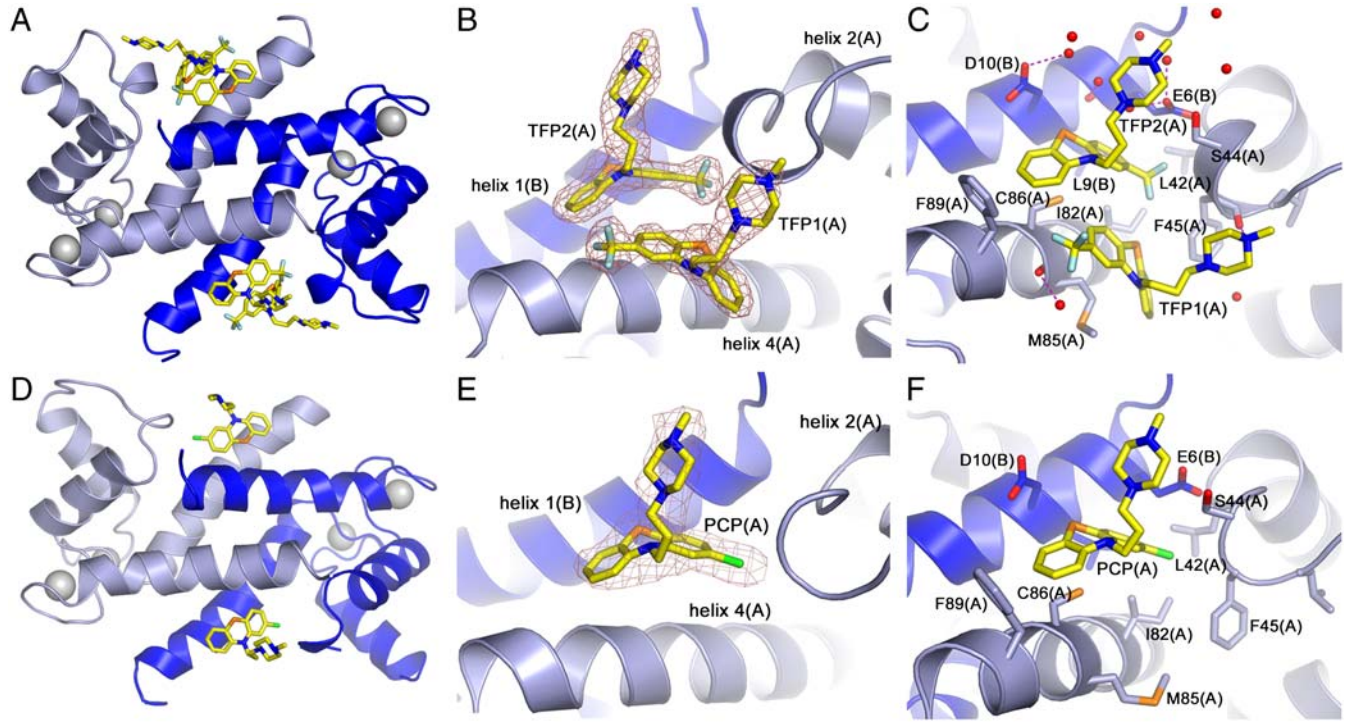

Fig. 3. Molecular interactions of Ca^{2+}-S100A4 and TFP or PCP. (*A*, *D*) Ribbon diagram of Ca^{2+}-S100A4/TFP and Ca^{2+}-S100A4/PCP AB dimer. Subunit A is *light blue*, subunit B is *dark blue*, and the TFP and PCP molecules are shown in *yellow*. Calcium ions are shown as *gray spheres*. (*B*, *E*) Zoomed view of TFP and PCP molecules in subunit A and their final refined 2Fo-Fc electron density map contoured at 1σ. (*C*, *F*). Molecular interactions of TFP and PCP molecules from subunit A. The water molecules are shown as *red spheres*. Hydrogen bonds are shown as *dashed pink lines*.

and the carboxylic group of Asp10(D), and one between the piperazine ring atom N2 and a water molecule (2.8 Å).

Based on AREAIMOL (23), interactions with the native AB dimer (including the TFP2(A) molecule) bury 58% of the solvent accessible area of TFP1(A) and 59% of the solvent accessible area of TFP2(A), whereas interactions with symmetry-related molecules (excluding waters) bury 29% and 40% of the solvent accessible area, respectively (Table S3). These values indicate that within the crystal, TFP-S100A4 interactions are strongly influenced by crystal contacts, which are propagated within each pentameric ring. In total, 81% of TFP1(A) (467 $Å^2$ out of 578 $Å^2$) and 87% of TFP2(A) (502 $Å^2$ out of 574 $Å^2$) solvent accessible areas are buried upon complex formation. Moreover, similar interactions are present in all the molecules in the asymmetric unit. However, the TFP1 and TFP2 molecules assume very different conformations within the S100A4 binding site (Fig. S1). Superimposition of the two molecules through their phenothiazine moieties reveals that the tricyclic rings have opposite puckers with respect to one another. Similarly, the piperazine rings, which are in a *chair* configuration, have opposing orientations.

Quaternary Structure of Ca^{2+}-S100A4/PCP. Similar to the Ca^{2+}-S100A4/TFP structure, PCP binding results in the assembly of five Ca^{2+}-S100A4/PCP dimers into a pentameric ring with a molecular point symmetry of 52 (Fig. S2*A*). However, the asymmetric unit of Ca^{2+}-S100A4/PCP contains only a single pentameric ring. Apparently, the different stoichiometry of PCP binding and crystallization conditions produced a unit cell with only half the volume of that observed for the Ca^{2+}-S100A4/TFP crystals. Otherwise, the structures of the Ca^{2+}-S100A4/TFP and Ca^{2+}-S100A4/PCP structures are similar with a rms deviation of 0.42 Å and 0.58 Å for all C^{α} atoms for monomers and pentameric rings, respectively.

Molecular Interactions Between PCP and Ca^{2+}-S100A4. In contrast to TFP, only a single high occupancy PCP molecule is present in each S100A4 subunit (two inhibitor molecules per dimer) (Fig. S2 *B*, *C*). The position and interactions of these high occupancy PCP molecules are almost identical to the TFP2 molecules (Fig. S2*D* and Fig. 3 *D*, *E*, *F*). PCP can be modeled with low occupancy in only two of the ten chains in the pentameric assembly at positions similar to those of TFP1.

Binding of TFP to Ca^{2+}-S100A4 and S100A4 Oligomerization. To determine whether the crystallographically observed interactions between the target binding cleft of S100A4 and TFP also occur in solution, we monitored perturbations of backbone ^{1}H-^{15}N chemical shifts as TFP was added to S100A4. The binding was Ca^{2+}-dependent as no chemical shift perturbations were detected when TFP was titrated into apo-S100A4. In the presence of Ca^{2+} and TFP, perturbations in ^{1}H-^{15}N correlations of Ca^{2+}-S100A4 were observed (>25 Hz) in the fast-exchange regime for residues in helix 1 (Leu5, Val11, Met12, and Lys18), loop 1 (Asn30), loop 2 (Leu42, Gly47, Arg49, and Asp51), helix 3 (Ala54, Phe55, Lys57, Leu58, and Met59), loop 3 (Glu69), and helix 4 (Leu79, Asn87, and Phe89) (Fig. S3). Several of the chemical shift perturbations are consistent with TFP binding to the hydrophobic target binding cleft of S100A4 that is exposed upon Ca^{2+}-binding. As the TFP concentration was increased to >350 μM, the Ca^{2+}-S100A4 resonances began to broaden and eventually disappeared, consistent with the formation of a large complex in solution.

To ascertain whether the S100A4/TFP oligomers observed by X-ray crystallography also occur in solution, we performed analytical sedimentation studies. Titration of Ca^{2+}-S100A4 with TFP resulted in the formation of a complex with a weight-average molecular weight of 133, 107 ± 8, 671 Da (Fig. 4*A*). An S100A4 oligomer comprised of five dimers and 20 TFP molecules has a calculated molecular weight of 124,123 Da, which is in good agreement with the experimentally determined molecular weight of the Ca^{2+}-S100A4/TFP oligomers. These observations suggest that under the conditions of our sedimentation studies, TFP induces a S100A4 oligomer similar to that observed by crystallography. Moreover, an examination of the Hill coefficient

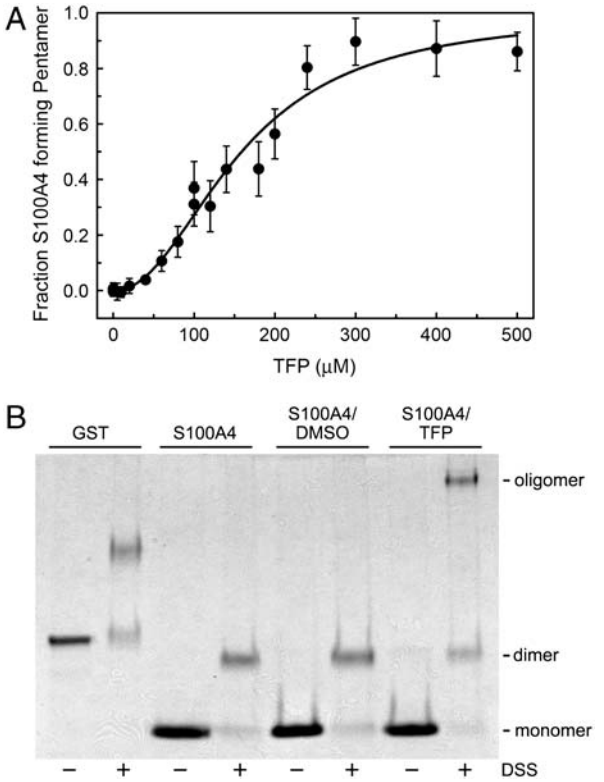

Fig. 4. TFP induces S100A4 oligomerization. (*A*) Plot of fraction S100A4 pentamer versus TFP concentration. Sedimentation equilibrium data were collected at 25 °C at a concentration of 80 μM S100A4 subunit. (*B*) Chemical cross-linking of Ca^{2+}-S100A4. Coomassie-stained SDS-PAGE of GST control, S100A4 alone, S100A4 + DMSO, and S100A4 + TFP. Monomeric and dimeric S100A4 have apparent molecular weights of approximately 11.5 kDa and 23 kDa, respectively.

($n_H = 2.4 \pm 0.3$) indicates that S100A4 oligomerization is cooperative with a midpoint of 150 μM TFP.

Since the sedimentation equilibrium experiments required significantly higher S100A4 subunit concentrations than those used to evaluate S100A4 activity in our biochemical assays, we used chemical cross-linking to examine whether TFP promotes S100A4 oligomerization under conditions in which S100A4 depolymerizes myosin-IIA filaments. In the presence of the chemical cross-linker disuccinimidylsuberate (DSS) (but no TFP), a prominent S100A4 band was detected at approximately 23 kDa, consistent with a dimer (Fig. 4*B*). In the presence of 100 μM TFP, a band of approximately 120 kDa was observed in the DSS-treated sample, which is consistent with the oligomer detected in sedimentation and X-ray studies. Larger oligomers were not detected by SDS-PAGE (Fig. S4*A*), suggesting the formation of a distinctly sized S100A4/TFP complex.

Sedimentation equilibrium analysis of this crosslinked species revealed a stable, homogenous S100A4 oligomer with a weight-average molecular weight of $143,372 \pm 7,462$ Da. DSS is a homobifunctional cross-linker that contains an amine-reactive *N*-hydroxysuccinimide ester at each end of an 8-carbon spacer arm. Typically the N terminus of the polypeptide chain and the lysine sidechain are the targets of DSS cross-linking. Each S100A4 subunit contains twelve lysine residues, all of which are solvent accessible. Given the uncertainty of the number of cross-links in the S100A4-TFP-DSS complex, the experimental molecular weight is in good agreement with the calculated molecular weight of an oligomer comprised of five S100A4 dimers, 20 TFP molecules, and multiple cross-links.

Our previous studies showed that under the conditions of our sedimentation assay approximately 75–80% of the myosin-IIA rods polymerize into filaments, and Ca^{2+}-dependent binding of S100A4 to myosin-IIA almost completely disassembles these preformed filaments (18 and 24). We also reported that 100 μM TFP completely blocks the ability of S100A4 to depolymerize myosin-IIA filaments (18). To test whether lower TFP concentrations were capable of inhibiting S100A4-mediated depolymerization of myosin-IIA filaments, we assayed a range of TFP concentrations in the promotion of disassembly assay. Concentrations of TFP up to 20 μM had no effect on S100A4's myosin-IIA depolymerizing activity (Fig. 5*A*). Only at TFP concentrations of ≥50 μM was significant inhibition of S100A4 activity detected. Notably, parallel cross-linking studies showed that at TFP concentrations that inhibit S100A4 activity, there is significant S100A4 oligomerization into high molecular weight complexes (Fig. 5*B*). In addition, the formation of large S100A4 oligomers by TFP requires Ca^{2+}-binding, as only S100A4 dimers were detected in the absence of calcium.

In our original screen against a library of FDA-approved drugs, we identified six phenothiazines as inhibitors of myosin-IIA associated S100A4 function. To determine if the TFP-induced oligomerization of S100A4 is specific to this phenothiazine, or is a general feature of this class of compounds, we performed chemical cross-linking assays under the same conditions utilized for TFP. All the phenothiazines tested, which include, flupenthixol, fluphenazine, chlorprothixene, prochlorperazine, and perphenazine induced S100A4 oligomerization, albeit to varying extents (Fig. S4*B*). Oligomeric S100A4 intermediates of 31, 46, and 66 kDa were observed for all of the phenothiazines. However, only chlorprothixene, and to a lesser extent prochlorperazine, induced the formation of large S100A4 oligomers (~120 kDa) as seen with TFP. The observation that 100 μM PCP does not promote the same

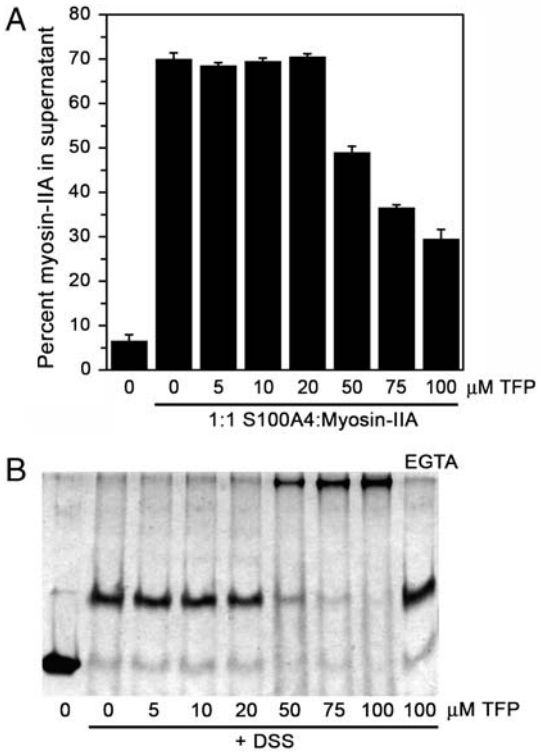

Fig. 5. S100A4-mediated myosin-IIA depolymerization in the presence of TFP. (*A*) Quantification of the myosin-IIA disassembly assay. In the absence of S100A4, 7% of the myosin-IIA rods are recovered in the supernatant; whereas in the presence of S100A4, 70% of the myosin-IIA rods are present in the supernatant. Values represent the mean ± sd from two independent experiments. (*B*) Chemical cross-linking of Ca^{2+}-S100A4 in the presence of increasing concentrations of TFP (0–100 μM). The *last lane* shows the products of the cross-linking reaction in the presence of EGTA and 100 μM TFP.

extent of oligomerization as TFP is consistent with our previous report that, 100 μM PCP inhibits S100A4's depolymerizing activity to a lesser extent than 100 μM TFP in the myosin-IIA disassembly assay (18), and, as evidenced by the S100A4/PCP structure, suggests that higher PCP concentrations are required to induce the formation of the pentameric S100A4 species.

Discussion

The current study represents one of the few examples of a S100-small molecule inhibitor structure, and provides a detailed description of a phenothiazine binding to an S100 protein. Previous studies reported on the Ca^{2+}-dependent interaction between S100A1/S100A1 (S100a), S100A1/S100B (S100a_0), and S100B/S100B (S100b) with TFP (25 and 26) as well as other phenothiazines (27), but did not delineate the binding site or residues involved in binding. Our studies demonstrate that each S100A4 subunit binds two TFP molecules in the target binding cleft formed by the hinge and helices 3 and 4.

In addition to the S100 proteins, other EF-hand containing proteins bind TFP. For example, troponin C binds two TFP molecules (PDB 1WRK) and calmodulin binds TFP with a range of stoichiometries; 1:1 (PDB 1CTR), 1:2 (PDB 1A29), and 1:4 (PDB 1LIN) (28–30). Even though S100A4, troponin C, and calmodulin are built upon the same basic four-helical structural module, the architectures of the TFP binding pockets, and the positions and orientations of the bound TFP molecules are quite different amongst the three proteins (Fig. 6). For example, in the Ca^{2+}-troponin C/TFP complex, the two TFP molecules are positioned deeper in the cleft formed by helices 3 and 4 due to the shorter loop between helices 2 and 3 and the lack of a second subunit (troponin C is a monomer) (Fig. 6*A*). Interestingly, in the crystal structure of the troponin C/TFP complex, dimerization occurs via interactions between the two pairs of TFP molecules, which "glue" the two troponin C monomers together. However, the disposition of the two troponin C subunits is quite different from that observed in a typical S100 family dimer. In the 1:2 Ca^{2+}-calmodulin/TFP complex (Fig. 6*B*), TFP1 binds deep in the cleft formed by the C-terminal EF-hand similar to troponin C, whereas TFP2 occupies an interdomain site. One consequence of TFP binding is to bring the N- and C-terminal domains of calmodulin together so that the protein assumes a compact globular conformation similar to that observed in structures of Ca^{2+}-calmodulin/peptide complexes (31 and 32). The compact structure of calmodulin prevents the two bound TFP molecules from clustering with TFP molecules from the symmetry-related protein chains.

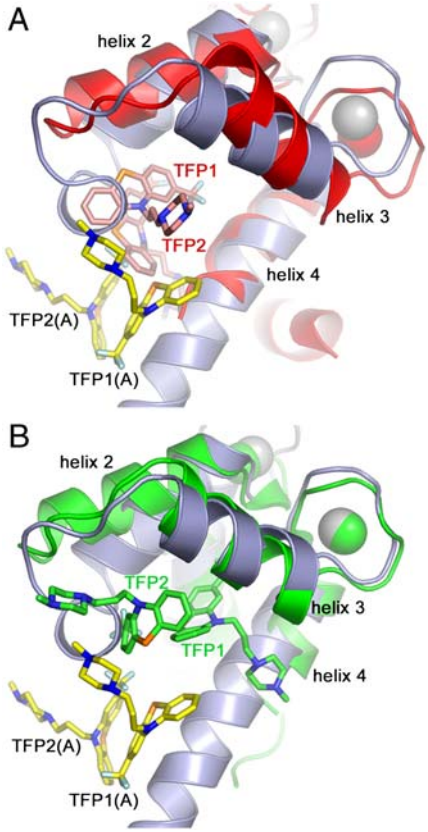

Fig. 6. Structural alignment of protein/TFP complexes. (*A*) Overlay of the Ca^{2+}-S100A4/TFP and troponin C/TFP complexes (PDB 1WRK). Subunit A of S100A4 is *light blue* and the TFP molecules are shown in *yellow*. Troponin C is *red* and the two bound TFP molecules are *light red*. Calcium atoms are presented as *corresponding colored spheres*. (*B*) Overlay of the Ca^{2+}-S100A4/TFP and calmodulin/TFP 1:2 complexes (PDB 1A29). Calmodulin and the two bound TFP molecules are *colored green*.

At present, S100A4 is the only EF-hand containing protein in which phenothiazines (TFP, PCP) induce the formation of higher-order oligomers. Both sedimentation equilibrium and chemical cross-linking studies demonstrate that Ca^{2+}-S100A4/TFP complexes can form oligomers comprised of at least five S100A4 dimers in solution. We previously reported that TFP binds to the Mero-S100A4 with an EC50 value of 55 ± 2.6 μM (18). Notably, our cross-linking experiments revealed that TFP concentrations of 50 μM are sufficient to induce S100A4 oligomerization and at this TFP concentration we first observe inhibition of S100A4's myosin-IIA-associated activities. Based on these findings, we propose that rather than directly competing with myosin-IIA, our structural, biophysical, and biochemical data support a model in which phenothiazines disrupt the S100A4/myosin-IIA interaction by sequestering S100A4 into a large well defined oligomer. A comparison of the residues that exhibit chemical shift perturbations following titration with TFP or the MIIA$^{1908–1923}$ peptide (5) indicates that the two ligands occupy overlapping, but nonidentical sites within the hydrophobic target binding cleft. (Table 1, Fig. S5*A*). While these observations might be consistent with the direct competition of TFP with the myosin-IIA peptide for S100A4 binding, it is important to note that disassembly assays use the physiologically relevant dimeric myosin-IIA coiled-coil that is also likely to be bivalent. Due to enhanced contact surface and avidity, the full-length myosin-IIA tail may not be easily displaced by TFP binding to S100A4.

An examination of available S100 protein/target peptide structures reveals that targets can bind in a variety of orientations and conformations (Fig. S5*B*). A hypothetical model of the S100A4/myosin-IIA pentamer suggests that inhibitor-induced oligomerization may preclude efficient recognition of the myosin-IIA coiled-coil due to unfavorable steric interactions. Myosin-IIA heavy chains bound to neighboring S100A4 subunits would cross inside the pentameric ring resulting in considerable steric clash (Fig. S6). In addition, the interior of the ring would have to accommodate an additional 35 residues from the C-terminal tailpiece of each myosin-IIA heavy chain (total 350 residues). Therefore, the totality of our data supports a more complex model in

Table 1. Comparison of chemical shift perturbations following addition of TFP or the MIIA$^{1908–1923}$ peptide to Ca^{2+}-S100A4 *.

Secondary structure	TFP	MIIA$^{1908–1923}$
helix 1	L5, ***V11***, ***M12***, L18	***V11***, ***M12***, S14, F16
pseudo EF-hand	***N30***	S20, F27, K28, ***N30***
loop 2 (hinge)	L42, ***G47***, R49, ***D51***	E41, ***G47***, K48, T50, ***D51***
helix 3	A54, F55, K57, L58, ***M59***	S60, L62
typical EF-hand	E69	N68, V70
helix 4	***L79***, N87, F89	F78, ***L79***, M85, C86
C-terminal loop	-	G92

*Shared residues are in bold italics.

which TFP may initially compete with myosin-IIA for the same binding pocket, but TFP-driven oligomerization prevents S100A4 binding to myosin-IIA. Additionally, the S100A4/PCP structure and the similar cross-linking behavior induced by a wide range of phenothiazines suggest that oligomerization is an important mechanistic feature of phenothiazine-induced S100A4 inhibition.

A number of small molecules have been described that inhibit protein function by altering the oligomerization equilibrium of the target protein. For example, a small molecule inhibitor of TNFα promotes subunit dissociation from the biologically active trimer to stabilize an inactive dimer (33). For porphobilinogen synthase, binding of the small molecule morphlock-1, shifts the oligomeric equilibrium from the active octamer to a low activity hexamer (34). In the case of HIV-1 integrase, inhibitory peptides shift the oligomerization equilibrium from the active dimer to an inactive tetramer (35). Although the inactive tetramer has not been characterized structurally, the peptide is thought to induce the formation of a nonnatural tetramer (35). The recent characterization of S100B, S100A8/A9 and S100A12 as well-defined oligomers comprised of two to four S100 dimers (20–22), suggests that the propensity to form higher-order structures may be a common feature of S100 proteins. This characteristic is also shared by S100A4 as we and others demonstrated that S100A4 can form tetramers or higher-order oligomers in the absence of added compounds (5 and 36). We propose that TFP-mediated oligomerization of S100A4 is another example of stabilization of an inactive, nonnatural oligomer. The formation of inactive S100A4 oligomeric assemblies may be a useful and unique strategy for inhibitor development.

Materials and Methods

Structure Determination. Recombinant human S100A4 was purified as described previously (24). Crystals of S100A4 bound to TFP or PCP were obtained by sitting drop vapor diffusion at 293 K. All structures were solved by molecular replacement and refined by standard methods, resulting in R_{cryst}/R_{free} values of 20.6%/25.9% and 25.2%/30.2% for the S100A4/TFP and S100A4/PCP complexes, respectively (Table S1). Details of the structure determination are provided in *SI text*.

NMR Spectroscopy. ^{1}H and ^{15}N resonances Ca^{2+}-S100A4 were followed during titrations with TFP at 37 °C using two-dimensional ^{1}H-^{15}N heteronuclear single quantum correlation (HSQC) spectra, and their assignments were confirmed with a three-dimensional ^{15}N-edited NOESY-HSQC experiment. Proton chemical shifts were reported with respect to the H_2O or HDO signal taken as 4.658 ppm relative to external trimethylsilyl-2,2,3,3-tetradeuteropropionic acid (TSP) (0.0 ppm), and the ^{15}N chemical shifts were indirectly referenced as described previously using the following ratio of the zero-point frequency: 0.10132905 for ^{15}N to ^{1}H. Details are provided in *SI text*.

Biochemical Assays. Promotion of disassembly assays were performed as described previously (24). S100A4 cross-linking experiments with performed at 25 °C with 5 mM disuccinimidylsuberate and 100–500 μM phenothiazines. Details are provided in *SI text*.

Analytical Ultracentrifugation. Sedimentation equilibrium experiments were performed at 25 °C with a Beckman XL-I analytical ultracentrifuge using the absorbance optics and Ti60 rotor. Details are provided in the *SI text*.

ACKNOWLEDGMENTS. We acknowledge the staff of the LRL Collaborative Access Team beamline at the Advanced Photon Source and the X29 beamline at the National Synchrotron Light Source. This work was supported with National Institutes of Health Grants CA129598 (to A.R.B.), and GM58888 and CA107331 (to D.J.W.). We acknowledge support from the Albert Einstein College of Medicine Cancer Center (National Cancer Institute (NCI) Grant P30CA13330).

1. Marenholz I, Heizmann CW, Fritz G (2004) S100 proteins in mouse and man: from evolution to function and pathology (including an update of the nomenclature). *Biochem Biophys Res Commun* 322:1111–1122.
2. Zimmer DB, Cornwall EH, Landar A, Song W (1995) The S100 protein family: history, function, and expression. *Brain Res Bull* 37:417–429.
3. Drohat AC, Baldisseri DM, Rustandi RR, Weber DJ (1998) Solution structure of calcium-bound rat S100B(betabeta) as determined by nuclear magnetic resonance spectroscopy. *Biochemistry* 37:2729–2740.
4. Sastry M, et al. (1998) The three-dimensional structure of Ca(2+)-bound calcyclin: implications for Ca(2+)-signal transduction by S100 proteins. *Structure* 6:223–231.
5. Malashkevich VN, et al. (2008) Structure of Ca2+-bound S100A4 and its interaction with peptides derived from nonmuscle myosin-IIA. *Biochemistry* 47:5111–5126.
6. Heizmann CW, Ackermann GE, Galichet A (2007) Pathologies involving the S100 proteins and RAGE. *Subcell Biochem* 45:93–138.
7. Helfman DM, Kim EJ, Lukanidin E, Grigorian M (2005) The metastasis associated protein S100A4: role in tumour progression and metastasis. *Br J Cancer* 92:1955–1958.
8. Garrett SC, Varney KM, Weber DJ, Bresnick AR (2006) S100A4, a mediator of metastasis. *J Biol Chem* 281:677–680.
9. Schneider M, Hansen JL, Sheikh SP (2008) S100A4: a common mediator of epithelial-mesenchymal transition, fibrosis and regeneration in diseases?. *J Mol Med* 86:507–522.
10. Grigorian M, Ambartsumian N, Lukanidin E (2008) Metastasis-inducing S100A4 protein: implication in non-malignant human pathologies. *Curr Mol Med* 8:492–496.
11. Kriajevska MV, et al. (1994) Non-muscle myosin heavy chain as a possible target for protein encoded by metastasis-related mts-1 gene. *J Biol Chem* 269:19679–19682.
12. Takenaga K, et al. (1994) Binding of pEL98 protein, an S100-related calcium-binding protein, to nonmuscle tropomyosin. *J Cell Biol* 124:757–768.
13. Watanabe Y, et al. (1993) Calvasculin, as a factor affecting the microfilament assemblies in rat fibroblasts transfected by src gene. *FEBS Lett* 324:51–55.
14. Kriajevska M, et al. (2002) Liprin beta 1, a member of the family of LAR transmembrane tyrosine phosphatase-interacting proteins, is a new target for the metastasis-associated protein S100A4 (Mts1). *J Biol Chem* 277:5229–5235.
15. Grigorian M, et al. (2001) Tumor suppressor p53 protein is a new target for the metastasis-associated Mts1/S100A4 protein: functional consequences of their interaction. *J Biol Chem* 276:22699–22708.
16. Semov A, et al. (2005) Metastasis-associated protein S100A4 induces angiogenesis through interaction with Annexin II and accelerated plasmin formation. *J Biol Chem* 280:20833–20841.
17. Dukhanina EA, et al. (2009) Opposite roles of metastasin (S100A4) in two potentially tumoricidal mechanisms involving human lymphocyte protein Tag7 and Hsp70. *Proc Natl Acad Sci USA* 106:13963–13967.
18. Garrett SC, et al. (2008) A biosensor of S100A4 metastasis factor activation: inhibitor screening and cellular activation dynamics. *Biochemistry* 47:986–996.
19. Laskowski R, MacArthur M, Moss D, Thornton J (1993) PROCHECK: a program to check the stereochemical quality of protein structures. *J Appl Crystallogr* 26:283–291.
20. Ostendorp T, et al. (2007) Structural and functional insights into RAGE activation by multimeric S100B. *Embo J* 26:3868–3878.
21. Korndorfer IP, Brueckner F, Skerra A (2007) The crystal structure of the human (S100A8/S100A9)2 heterotetramer, calprotectin, illustrates how conformational changes of interacting alpha-helices can determine specific association of two EF-hand proteins. *J Mol Biol* 370:887–898.
22. Moroz OV, Blagova EV, Wilkinson AJ, Wilson KS, Bronstein IB (2009) The crystal structures of human S100A12 in apo form and in complex with zinc: new insights into S100A12 oligomerisation. *J Mol Biol* 391:536–551.
23. Collaborative Computational Project N (1994) The CCP4 suite: programs for protein crystallography. *Acta Crystallogr D* 50:760–763.
24. Li ZH, Spektor A, Varlamova O, Bresnick AR (2003) Mts1 regulates the assembly of nonmuscle myosin-IIA. *Biochemistry* 42:14258–14266.
25. Pingerelli PL, Mizukami H, Mooney MJ, Schlaepfer AL (1989) Spectral studies of the Ca2+-dependent interaction of trifluoperazine with S100b. *J Protein Chem* 8:183–196.
26. Pingerelli PL, Mizukami H, Wagner AS, Bartnicki DE, Oliver JP (1990) Investigation of the Ca2(+)-dependent interaction of trifluoperazine with S100a: a 19F NMR and circular dichroism study. *J Protein Chem* 9:169–175.
27. Marshak DR, Watterson DM, Van Eldik LJ (1981) Calcium-dependent interaction of S100b, troponin C, and calmodulin with an immobilized phenothiazine. *Proc Natl Acad Sci USA* 78:6793–6797.
28. Vertessy BG, et al. (1998) Simultaneous binding of drugs with different chemical structures to Ca2+-calmodulin: crystallographic and spectroscopic studies. *Biochemistry* 37:15300–15310.
29. Cook WJ, Walter LJ, Walter MR (1994) Drug binding by calmodulin: crystal structure of a calmodulin-trifluoperazine complex. *Biochemistry* 33:15259–15265.
30. Vandonselaar M, Hickie RA, Quail JW, Delbaere LT (1994) Trifluoperazine-induced conformational change in Ca(2+)-calmodulin. *Nat Struct Biol* 1:795–801.
31. Ikura M, et al. (1992) Solution structure of a calmodulin-target peptide complex by multidimensional NMR. *Science* 256:632–638.
32. Meador WE, Means AR, Quiocho FA (1993) Modulation of calmodulin plasticity in molecular recognition on the basis of X-ray structures. *Science* 262:1718–1721.
33. He MM, et al. (2005) Small-molecule inhibition of TNF-alpha. *Science* 310:1022–1025.
34. Lawrence SH, et al. (2008) Shape shifting leads to small-molecule allosteric drug discovery. *Chem Biol* 15:586–596.
35. Hayouka Z, et al. (2007) Inhibiting HIV-1 integrase by shifting its oligomerization equilibrium. *Proc Natl Acad Sci USA* 104:8316–8321.
36. Gingras AR, et al. (2008) Crystal structure of the Ca(2+)-form and Ca(2+)-binding kinetics of metastasis-associated protein, S100A4. *FEBS Lett* 582:1651–1656.